Angewandte Zuschriften

Controlled Release

DOI: 10.1002/ange.201207986

Photothermally Activated Hybrid Films for Quantitative Confined Release of Chemical Species**

Paolo Matteini, Francesca Tatini, Lapo Luconi, Fulvio Ratto, Francesca Rossi, Giuliano Giambastiani, and Roberto Pini**

Nanophotonic solutions are providing new answers to topical biomedical challenges. A relevant example is the use of laser-activated plasmonic nanoparticles for the generation of heat.[1] These are nanosized metallic structures with unique optical properties, which originate from sharp plasmonic resonances, that is, collective oscillations of conduction-band electrons at optical frequencies. These oscillations may be driven by light from, for example, a laser source, which provides intense photothermal conversion.[2] This feature is being exploited for a variety of biomedical applications[3] including cancer therapy, molecular signaling, drug delivery, and bond activation.[4–6]

Herein we exploit these materials to implement a method for dose- and space-controlled chemical release from photo-activated nanocomposite films. For light absorption gold nanorods (NRs) were employed. These are a convenient choice of plasmonic nanoparticle featuring extremely efficient photothermal conversion in the so-called therapeutic window, that is, the spectral slot from 700 to 1300 nm where principal biological components (water, melanin, etc.) and common exogenous chromophores exhibit the highest optical transparency.[2,7] We used small $((40\pm6)\,\text{nm}\times(10\pm2)\,\text{nm})$, 3.9 ± 0.5 aspect ratio NRs (Figure 1 a, Supporting Information Figure S1a), whose photothermal response has been discussed in previous papers,[5,8] to ensure rapid and smooth thermalization with their surrounding environment. NRs were uniformly dispersed inside a porous chitosan film, which was conferred with unique optical properties including an absorption band around 820 nm and another weaker one around 540 nm, arising from separate plasmonic oscillations of the NRs (Figure 1 b). Its high versatility and biocompatibility make chitosan an ideal option for the fabrication of hybrid nanocomposite materials for applications in biomedicine, such as scaffolds for tissue engineering,[9] substrates for gene transfer,[10] and bioadhesives for tissue repair.[11] Moreover the structure of chitosan films can be tailor-made to provide interconnected internal micropores (Figure S2), to sustain the release of molecules to the outer environment.[12] The density of NRs in the film was optimized to avoid detrimental effects of plasmonic coupling (Figure S1b),[2] which could impair their photothermal conversion efficiency (Figure S1c). The controlled release of a chemical species on laser activation was provided by the addition of a thermosensitive reservoir inside the film. This reservoir was engineered

[*] Dr. P. Matteini, Dr. F. Tatini, Dr. F. Ratto, Dr. F. Rossi, Prof. R. Pini
Institute of Applied Physics "Nello Carrara"
National Research Council
via Madonna del Piano 10, 50019 (Italy)
E-mail: p.matteini@ifac.cnr.it
r.pini@ifac.cnr.it
Dr. L. Luconi, Dr. G. Giambastiani
Institute of Chemistry of Organometallic Compounds
National Research Council
via Madonna del Piano 10, 50019 (Italy)

[**] This work has been partially supported by the Project of the Health Board of the Tuscan Region "NANO-CHROM" and "IPERNANO" and by the Network of Excellence "Photonics 4 Life".

Supporting information for this article is available on the WWW under http://dx.doi.org/10.1002/anie.201207986.

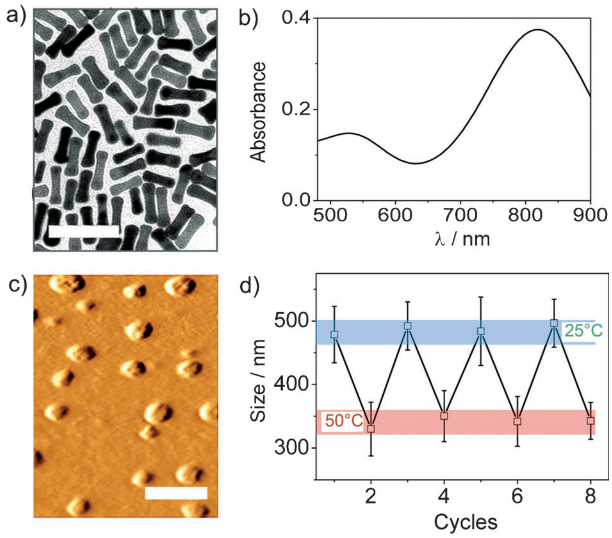

Figure 1. a) TEM image and b) absorption spectrum of the nanorods (NRs) used in the experiments (bar = 100 nm). c) AFM topography of the PCL-PEG-PCL micelles (bar = 1 μm). d) Cycles of micelle size contraction by switching the temperature from 25 °C to 50 °C.

to effectively retain functional molecules up to physiological temperature and to trigger their ejection upon a thermal stimulus. Because of their combination of suitable thermal response and good bioaffinity, we used functional block copolymers.[13] In an aqueous environment, these amphiphilic copolymers undergo rapid self-assembly in micelles with a hydrophobic core and a hydrophilic shell, with a final conformation that depends on the temperature.[14] In particular, we used micelles of poly(caprolactone-*b*-ethylene glycol-*b*-caprolactone) (PCL-PEG-PCL; Figure 1 c, S3a), which have been proposed for drug delivery applications because of their excellent payload properties.[15] These micelles were found to undergo a reversible approximately 35 % volume contraction once they have been exposed to a moderate thermal rise higher than the physiological values (Figure 1 d), owing to a phase transition at around 40 °C (Figure S3b), which is interpreted as a combination of PEG shell collapse and PCL core fusion at high temperatures.[16] Overall, the final formulation (Figure 2 a) consisted of an approximately 150 μm-thick flexible film with an optical absorber that generates heat upon activation by light, which stimulates the release of a chemical species from a contracting reservoir, the released species can then pass through the porous frame of the film (Figure 2 b–d).

Fine control over the photothermal process was required to realize temperatures within a window high enough to trigger sufficient activation of the reservoir but below a threshold temperature that would cause irreversible damage to cellular components.[17] On a timescale of a few minutes, these constraints define an operative interval approximately between 40 and 50 °C (Figure S4). Optimal results were obtained by using laser intensities in a range between 0.1 and 0.5 $\text{W}\,\text{cm}^{-2}$ from a continuous wave diode laser, with an emission wavelength (810 nm) overlapping the effective optical absorption of the NRs (see for example, Figure 3 a for $t_{irr} = 1$ min). With these irradiation conditions,

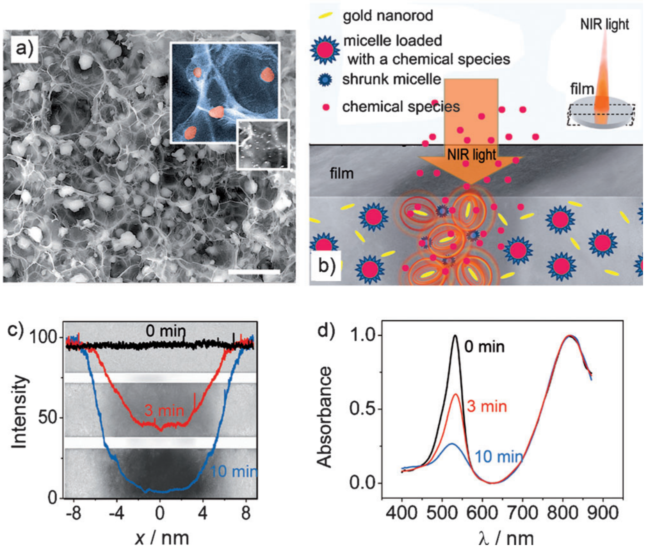

Figure 2. a) SEM micrographs of a film cross-section containing thermosensitive micelles organized mainly in clusters in the porous chitosan matrix (bar = 20 μm). Insets: false-color magnification to emphasize micelles (red) and back-scattered acquisition from a selected area showing NRs as bright spots. b) schematic representation of the functioning nanocomposite films. c,d) Fluorescence intensity profiles and absorbance spectra of a 4 mm irradiated area of a R6G-loaded film (0.32 W cm^{-2}) for 0 (black), 3 (red), or 10 (blue) minutes. The 820 nm band of the NRs remained constant, while the R6G peak at 529 nm decreased with irradiation time.

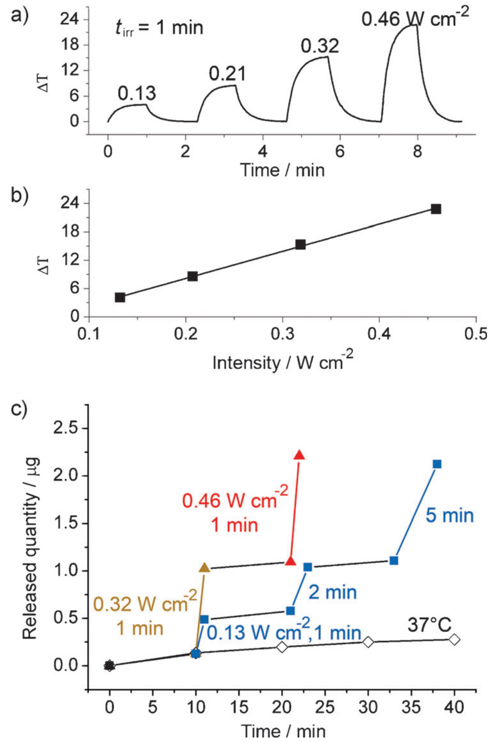

Figure 3. a) Temperature profiles obtained by illuminating a film sample with increasing laser intensities (0.13, 0.21, 0.32, 0.46 W cm^{-2}, t_{irr} = 1 min). b) Maximum temperature increase from (a) versus laser intensity. c) Tests of R6G release with different cycles: ▲: 10 min at 37 °C, 1 min at 0.32 W cm^{-2}, 10 min at 37 °C, 1 min at 0.46 W cm^{-2}; ■: 10 min at 37 °C, 1 min at 0.13 W cm^{-2}, 10 min at 37 °C, 2 min at 0.13 W cm^{-2}, 10 min at 37 °C, 5 min at 0.13 W cm^{-2}; ◇: release at 37 °C.

Figure 3 b reveals a clear linear relationship between intensity and temperature, which enabled a precise modulation of the extent of the photothermal conversion. We believe that this behavior is favored by the high photobleaching threshold of the NRs (see Figure 2 d).[2] In turn, an accurate temperature setting provided consistency and control over dosing the chemical release, which was proved to be a function of the light intensity and irradiation time (Figure 3 c).

In our groundwork we investigated the release of common dyes to mammalian cells and tissues. A film sample was placed in contact with a cell monolayer, which was chosen as a representative model of biological substrate. Prior to its incubation with cells, the film sample was loaded with the rhodamine 6G (R6G) fluorophore, which has the potential to become internalized in intracellular compartments. By varying the light intensity in the range between 0.15 and 0.54 W cm^{-2}, we observed the formation of fluorescence patterns, which occurred in the part of the cell monolayer in contact with the irradiated portion of the film (4 mm laser spot size, t_{irr} = 1 min; Figure 4 a,d and S7). The confinement of the fluorescence stain largely within the spot irradiated by the laser, for laser intensities around 0.25 W cm^{-2} (Figure 4 d), that is, well below the threshold of irreversible cell damage (0.45 W cm^{-2}, Figure 4 b), inspired us to pursue the precise spatial control of this minimally invasive marking process. This result is interpreted as being a consequence of a transient hyperpermeability of cell membranes when physiological temperatures are exceeded (Figure S5 and Ref. [18]). When approaching certain time and temperature thresholds (e.g., 42 °C for a 1 min, see Figure S5), the plasmatic membrane permeability begins to grow, which was not seen to induce significant cell death until about 50 °C and 10 min (Figure S4). Meanwhile, this process may be exploited to promote an accumulation of chemical species within intracellular compartments.[19] Therefore the controlled temperature increase in the cell monolayer in contact with the irradiated film induces a preferential internalization of the released molecules, which happens to be mostly confined within the irradiated area, particularly in the case of the optimal intensity, 0.25 W cm^{-2}. At significantly higher intensities, heat diffusion (Figure S7c,S8) causes a progressive expansion of the portion of stained cells with respect to the spot under irradiation (Figure S7a). These preliminary tests provide a proof of concept and parameterization for the efficient and selective release of a chemical species to a cell monolayer from laser-activated nanocomposite films. This method may involve developments for biomedical and health care applications, as well as in other contexts. Some of these perspectives are outlined as follows:

After a preliminary parameterization, we extended our experiments by using a configuration in which the film was activated by a focused laser beam, to release its contents in selected areas of a variety of animal tissues, including ophthalmic and gastrointestinal samples. By modulating the irradiation conditions in agreement with the temperature dynamics as above and with the particular optical properties

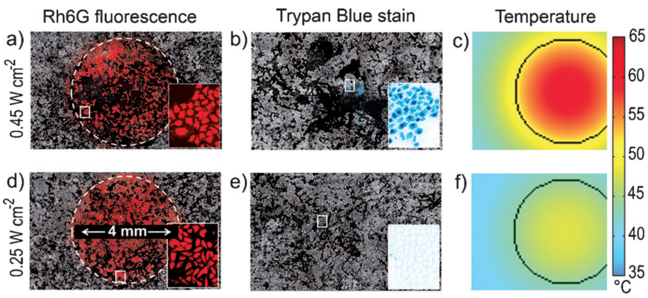

Figure 4. Marking of a cell monolayer by selective uptake of R6G released from a laser-illuminated area (4 mm size) of an overlying film at different intensities (a–c: 0.45 $W cm^{-2}$; d–f: 0.25 $W cm^{-2}$; $t_{irr}=1$ min). a,d) R6G fluorescence patterns. b,e) Evidence of cell death (trypan blue stain) and detachment from dish surface. c,f) Calculated temperature distribution during irradiation. Images size: (6.7×4) mm^2. Inset images are 10× magnifications of selected areas.

of those biological tissues under examination, we obtained a similar confined stamping of cellular areas where the film was exposed to light (Figure 5 a–c). This observation indicates the use of the proposed method for marking cells with the spatial control provided by the light spot size and a dosage that may be predetermined by modulation of the relevant irradiation parameters. These features may be of interest, for example, for developing advanced and personalized pharmacological therapies, in which a precise release of drugs to specific body regions (e.g. a tumor site) is required.

Afterwards, in an attempt to evaluate the relevance of this method in applications which may transcend its therapeutic use, we tested the possibility of achieving accurate marking of external soft tissues (Figure 5 d–f). A variety of shapes was found to be precisely replicated onto the epidermal layer of skin specimens by using stencils of different profiles as shadow masks before selected film areas. We envision that such an approach may find application in a variety of aesthetic treatments, such as body painting and minimally invasive tattooing.

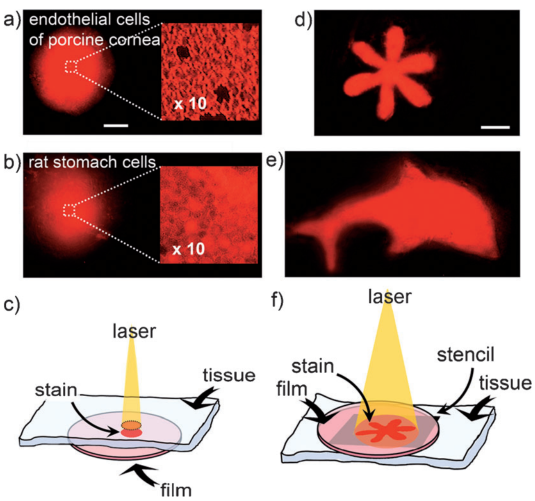

Figure 5. Marking of biological tissues by light-activation of R6G-loaded films placed in contact with them. Confined regions of endothelial cells from a porcine cornea (a) and rat stomach cells (b) are stained by delivering the laser energy (a: 0.31 $W cm^{-2}$, b: 0.38 $W cm^{-2}$ and 1 min) to a 1 mm diameter spot on the film as shown in (c) (bar = 0.5 mm). Insets: 10× magnification of selected regions. d, e) Fluorescent patterns transferred onto the epidermal layer of rat skin samples by illuminating (0.24 $W cm^{-2}$, 5 min) a 10 mm diameter spot of a film through stencils positioned at the film/tissue interface as shown in (f) (bar = 1 mm).

In conclusion, we have set up a new method for releasing functional molecules to living cells and tissues in a dose- and spatio-controlled manner. The release effect rests on a cascade process, which is triggered by remote light stimulation of a nanocomposite film comprising an optical absorber and a thermosensitive reservoir in a polymeric porous frame. This method may generate a variety of different opportunities, such as the confined staining of cell cultures, highly controlled and localized pharmacological therapies, as well as the development of innovative and minimally invasive health care and aesthetic treatments.

Experimental Section

Low-molecular weight chitosan (Sigma–Aldrich) was dissolved in an aqueous NRs dispersion, which was obtained by an autocatalytic wet-chemistry method,[8,20] up to a 3.5% w/v final concentration (see details in Supporting Information). After purification, the mixture was equilibrated for 12 h at 40°C. Then 50 μL of an ethanol solution of PCL-PEG-PCL copolymer (30% wt, poly(ethylene glycol) (PEG); poly(ε-caprolactone) (PCL)) were rapidly injected into 150 μL of the NRs-chitosan composite and mixed until completely homogenized. For the release measurements, the PCL-PEG-PCL solution included a 1 $mg mL^{-1}$ content of R6G. Lastly 30 μL of this solution were poured into 0.5 cm^2 polystyrene molds and, after 60 min solvent evaporation under controlled conditions (25°C, N_2 flux), insolubilized by treatment with NaOH 1 M, followed by abundant rinsing with ultrapure water. Film samples were stored at 4°C until further investigation. The optical properties of the samples were investigated using a Jasco V-560 spectrophotometer. The ultrastructure of freeze-dried samples was inspected by using a Fei Quanta 200 environmental SEM, operated at 25 kV under standard high-vacuum conditions. A detector of backscattered electrons was used to detect the NRs distribution. AFM analysis of micelles obtained from a 1 $mg mL^{-1}$ PCL-PEG-PCL aqueous solution and deposited on a mica substrate was carried out on a Quesant Q-Scope 250 instrument operated in tapping mode. Dynamic light scattering (DLS) was performed on a zeta potential/particle sizer (Malvern Nano ZS90) to determine the distribution of the hydrodynamic diameters of micelles.

The temperature developed by the films during a photothermal assay was measured from the opposite side to the one under direct irradiation by using an infrared thermocamera (Thermovision A20 FLIR Systems Inc.). The release of R6G from the films was investigated by incubating each sample in PBS (pH 7.4) at 37°C, followed by exposure to laser light for different time intervals and light fluences. The buffer solution around the film was collected and replaced with fresh PBS every 10 min or after each dose of light stimulation. Human HeLa cells were cultured in phenol-red-free Dulbecco's modified Eagle medium (DMEM) supplemented with 10% fetal bovine serum (FBS), 1 mM glutamine, 100 $U mL^{-1}$ penicillin, and 100 $\mu g mL^{-1}$ streptomycin in a 5% CO_2 humidified atmosphere at 37°C. For the laser experiments, cell seeding was carried out in 33 mm-size polystyrene petri dishes until reaching a confluence of 80–90%. A description of the bench setups used for the laser experiments and temperature measurements is given in Supporting Information. An 810 nm wavelength light from an AlGaAs diode laser (El.En S.p.A.) running in continuous wave mode was employed for all measurements. 4 h after the laser treatment, cell death was checked by staining with trypan blue (Sigma Aldrich). Dead cells absorb the dye and take a blue appearance. The temperature distribution inside and around the irradiated spots was calculated using a two-dimensional mathematical model based on the solution of the bio-heat equation through the Finite Element Method (Comsol Multiphysics, Comsol AB), as described in Supporting Information. Images of R6G uptake were acquired by a Leica DMI3000B inverted microscope with a green (515–560 nm) excitation coupled with a 580 nm dichroic mirror and a long pass (LP590) filter. Phase-contrast micrographs of the same regions were used as background after thresholding in composite images to emphasize the local distribution of the fluorochrome. Additional experiments were performed on freshly explanted animal tissues. In this case, a film was placed in contact with a tissue sample and irradiated with a laser platform similar to that for cell cultures (Figure S4).

Received: October 3, 2012
Revised: March 12, 2013
Published online: May 9, 2013

Keywords: gold nanorods · light-sensitive materials · micelles · nanophotonics · photothermal conversion

[1] a) J. A. Schuller, E. S. Barnard, W. Cai, Y. C. Jun, J. S. White, M. L. Brongersma, *Nat. Mater.* **2010**, *9*, 193–204; b) J. K. Young, E. R. Figueroa, R. A. Drezek, *Ann. Biomed. Eng.* **2012**, *40*, 438–459.
[2] H. Huang, S. Neretina, M. A. El-Sayed, *Adv. Mater.* **2009**, *21*, 4880–4910.
[3] a) P. K. Jain, X. H. Huang, I. H. El-Sayed, M. A. El-Sayed, *Acc. Chem. Res.* **2008**, *41*, 1578–1586; b) L. Dykman, N. Khlebtsov, *Chem. Soc. Rev.* **2012**, *41*, 2256–2282; c) M. F. Bédard, D. Braun, G. B. Sukhorukov, A. G. Skirtach, *ACS nano* **2008**, *2*, 1807–1816; d) R. Huschka, J. Zuloaga, M. W. Knight, L. V. Brown, P. Nordlander, N. J. Halas, *J. Am. Chem. Soc.* **2011**, *133*, 12247–12255.
[4] a) S. Lal, S. E. Clare, N. J. Halas, *Acc. Chem. Res.* **2008**, *41*, 1842–1851; b) L. E. Strong, J. L. West, *Wiley Interdiscip. Rev. Nanomed. Nanobiotechnol.* **2011**, *3*, 307–317.
[5] G. von Maltzahn, J. H. Park, K. Y. Lin, N. Singh, C. Schwoppe, R. Mesters, W. E. Berdel, E. Ruoslahti, M. J. Sailor, S. N. Bhatia, *Nat. Mater.* **2011**, *10*, 545–552.
[6] a) P. Matteini, F. Ratto, F. Rossi, S. Centi, L. Dei, R. Pini, *Adv. Mater.* **2010**, *22*, 4313–4316; b) P. Matteini, F. Ratto, F. Rossi, R. Pini, *J. Biomed. Opt.* **2012**, *17*, 010701; c) T. B. Huff, L. Tong, Y. Zhao, M. N. Hansen, J. X. Cheng, A. Wei, *Nanomedicine* **2007**, *2*, 125–132; d) M. Bikram, A. M. Gobin, R. E. Whitmire, J. L. West, *J. Controlled Release* **2007**, *123*, 219–227; e) M. S. Yavuz, Y. Cheng, J. Chen, C. M. Cobley, Q. Zhang, M. Rycenga, J. Xie, C. H. Kim, K. H. Song, A. G. Schwartz, L. V. Wang, Y. Xia, *Nat. Mater.* **2009**, *8*, 935–939.
[7] J. Perez-Juste, I. Pastoriza-Santos, L. M. Liz-Marzan, P. Mulvaney, *Coord. Chem. Rev.* **2005**, *249*, 1870–1901.
[8] F. Ratto, P. Matteini, F. Rossi, L. Menabuoni, N. Tiwari, S. K. Kulkarni, R. Pini, *Nanomedicine* **2009**, *5*, 143–151.
[9] V. M. Rusu, C. H. Ng, M. Wilke, B. Tiersch, P. Fratzl, M. G. Peter, *Biomaterials* **2005**, *26*, 5414–5426.
[10] H. Shen, J. Tan, W. M. Saltzman, *Nat. Mater.* **2004**, *3*, 569–574.
[11] a) S. Ladet, L. David, A. Domard, *Nature* **2008**, *452*, 76–79; b) P. Matteini, F. Ratto, F. Rossi, G. rossi, G. Esposito, A. Puca, A. Albanese, G. Maira, R. Pini, *J. Biomed. Opt.* **2010**, *15*, 041508; c) P. Matteini, F. Ratto, F. Rossi, M. de Angelis, L. Cavigli, R. Pini, *J. Biophotonics* **2012**, *5*, 868–877.
[12] N. Bhattarai, J. Gunn, M. Q. Zhang, *Adv. Drug Delivery Rev.* **2010**, *62*, 83–99.
[13] a) M. A. C. Stuart, W. T. S. Huck, J. Genzer, M. Muller, C. Ober, M. Stamm, G. B. Sukhorukov, I. Szleifer, V. V. Tsukruk, M. Urban, F. Winnik, S. Zauscher, I. Luzinov, S. Minko, *Nat. Mater.* **2010**, *9*, 101–113; b) D. Schmaljohann, *Adv. Drug Delivery Rev.* **2006**, *58*, 1655–1670.
[14] a) N. Rapoport, *Prog. Polym. Sci.* **2007**, *32*, 962–990; b) M. Talelli, W. E. Hennink, *Nanomedicine* **2011**, *6*, 1245–1255.
[15] S. Zhou, X. Deng, H. Yang, *Biomaterials* **2003**, *24*, 3563–3570.
[16] S. J. Bae, J. M. Suh, Y. S. Sohn, Y. H. Bae, S. W. Kim, B. Jeong, *Macromolecules* **2005**, *38*, 5260–5265.
[17] M. H. Niemz, *Laser—Tissue Interactions*, Springer, Berlin, **1996**.
[18] J. C. Bischof, J. Padanilam, W. H. Holmes, R. M. Ezzell, R. C. Lee, R. G. Tompkins, M. L. Yarmush, M. Toner, *Biophys. J.* **1995**, *68*, 2608–2614.
[19] a) P. Wust, B. Hildebrandt, G. Sreenivasa, B. Rau, J. Gellermann, H. Riess, R. Felix, P. M. Schlag, *Lancet Oncol.* **2002**, *3*, 487–497; b) P. Matteini, M. R. Martina, G. Giambastiani, F. Tatini, R. Cascella, F. Ratto, C. Cecchi, G. Caminati, L. Dei, R. Pini, *J. Mater. Chem. B* **2013**, *1*, 1096–1100.
[20] B. D. Busbee, S. O. Obare, C. J. Murphy, *Adv. Mater.* **2003**, *15*, 414–416.

